Improving Balancing Activation Through Continuous-Time Optimization and Increased Market Time-Resolution

1st Vegard Viken Kallset
Department of Electric Energy
Norwegian University of Science and Technology
Trondheim, Norway
vegard.v.kallset@ntnu.no

2nd Hossein Farahmand
Department of Electric Energy
Norwegian University of Science and Technology
Trondheim, Norway
hossein.farahmand@ntnu.no

***Abstract*—The Nordic power system and the Core region in Europe are transitioning from an hourly to a 15-minute time resolution in the day-ahead electricity market by 2025. This change aims to reduce structural imbalances caused by mismatches between discrete power schedules and continuously varying demand, which lead to inefficient reserve activation, frequency deviations, and increased balancing costs.**

In this paper, we employ a two-stage stochastic unit commitment model for market clearing and compare the results of the balancing stage with a continuous-time balancing approach. Additionally, we evaluate the impact of increasing time resolution and assess whether further granularity provides additional benefits.

Our results show that higher time resolution and continuous modeling reduce the need for balancing reserves by better approximating real load variations. These findings provide valuable insights for system operators to improve power plant ramping strategies and reserve allocation, ultimately enhancing system stability and reducing operational costs in future power systems.

***Index Terms*—Continuous-time optimization, real-time system balancing, structural imbalances**

I. Introduction

The Nordic power system, alongside the Core region in Europe, is undergoing a major shift in its electricity market design. In 2025, the time resolution of the day-ahead market will change from hourly to 15-minute intervals [1]. This transition aims to mitigate so-called structural imbalances: systematic deviations between planned generation and actual demand that occur due to the mismatch between discrete power schedules and continuously varying electricity demand.

As the power system changes to finer time resolutions, the task of activating the balancing reserves should also become more automated and proactive [2]. While Frequency Containment Reserves (FCR) react instantly and Automatic Frequency Restoration Reserves (aFRR) should be fully activated within 10 minutes, Manual Frequency Restoration Reserves (mFRR) can take up to 15 minutes to ramp up. To be ready for unforeseen imbalances, the system operator should conserve the fastest reserves as much as possible and use slower reserves to handle predictable imbalances [3].

Traditional discrete unit-commitment (UC)-based market-clearing (MC) models often yield generation schedules that do not efficiently manage the flexibility of generating units and fail to reserve sufficient balancing capacity [4].

Continuous-time optimization represents power system variables through weights on continuous basis-functions rather than discrete steps, resulting in smoother operation curves [5]. This approach has evolved from thermal systems [5] to multi-stage stochastic reserve and unit commitment models [6] and further to cascaded hydropower systems [7].

Previous work has shown that fixing unit-commitment variables from discrete models in continuous frameworks can lead to load shedding and, thus higher total system costs [8].

In this work, we aim to examine the impact of different time resolutions in both discrete and continuous optimization models by using an approach similar to [8]. Rather than looking at total system costs, we evaluate the total balancing activation needs of both models. This metric offers a more equitable comparison and demonstrates the practical benefits of continuous optimization in reducing structural imbalances.

Our research makes two specific contributions: First, we provide a quantitative assessment of how continuous-time optimization reduces the need for balancing activation by better approximating real load variations. Second, we analyze the impact of increased time resolution on both modeling paradigms and quantify the remaining potential for the reduction of structural imbalances that could be achieved by increasing time resolution further.

The remainder of this paper is organized as follows: Section II presents the mathematical formulation, Section III describes the case study and analyzes the impacts of different time resolutions on balancing needs and model accuracy. Finally, section IV provides concluding remarks.

II. Methods

This section presents the mathematical formulation of our two approaches: a discrete two-stage stochastic unit

Parameters:

D_{at}, $\bar{D}_{ats}$	First/second stage demand
C_p	Variable cost of production [mu/MW]
C_p^R	Cost of procuring reserve capacity [mu/MW]
C_a	Cost of balancing activation [mu/MW]
C^s, C^d	Cost of shedding load/dumping power [mu/MW]
C_p^{SU}	Cost of dumping power [mu/MW]
$C^{\uparrow}$, $C^{\downarrow}$	Cost of upward/downward activation [mu/MW]
E_p	Energy conversion factor [MWs/m^3]
Q_{pt}^{nat}	Natural inflow [m^3/s]
Q_p^{max}	Maximal flow out of reservoir [m^3/s]
V_p^{init}	Initial reservoir volume [m^3]
V_p^{max}	Maximal reservoir capacity [m^3]
P_p^{min}, P_p^{max}	Min/max production [MW]
$\hat{P}_{ptsb}^{Min}$, $\hat{P}_{ptsb}^{Min}$	Min/Max production for continuous model
F^{max}	Maximum flow on transmission line
$R^{\downarrow}$, $R^{\uparrow}$	Up/down buffer reserve capacity [MW]
π	Scenario probability

Sets:

S	Scenarios, s
T	Time periods, t
A	Areas, a
P_a^{area}	Power plants in area, p
P^T	Thermal power plants, p
P^H	Hydro power plants, p
I_p	Plants with outlets into a given hydro plant, p
L	Set of all transmission lines l
L_a	Set of all transmission lines connect to area a l
B	Set of Bernstein basis polynomials b

Variables:

$g_{p,t}$,$\bar{g}_{p,t,s}$	First/second stage production [MW]
$r_{pt}^{\downarrow}$, $r_{pt}^{\uparrow}$	Down/up balancing capacity [MW]
$a_{pts}^{\downarrow}$, $a_{pts}^{\uparrow}$	Down/up balancing activation [MW]
q_{pt}^{out}, $\bar{q}_{pt}^{out}$	First/second stage flow out of reservoir [m^3/s]
q_{pt}^{in}, $\bar{q}_{pt}^{in}$	First/second stage flow into reservoir [m^3/s]
v_{pt}, $\bar{v}_{pts}$	First/second stage reservoir volume [m^3]
s_{tas}^{+}	Load shedded [MW]
s_{tas}^{-}	Power dumped [MW]
b_{pt}	Binary, 1 if power plant is on in timestep t
SU_{pt}	Binary, 1 if power plant p turns on in timestep t
f_{lt}, $\bar{f}_{lts}$	First/second stage flow on line l

commitment model and a continuous-time optimization model that replaces only its second stage. We first introduce the shared objective function (1), then detail the discrete model's constraints for both stages, and finally describe how the continuous model interfaces with the discrete model.

Equation (1) gives the objective function, which minimizes the total system costs, including variable production costs, balancing reservation costs, balancing activation costs, load shedding costs, and power dumping costs.

$$\begin{aligned}\min \quad & \sum_{t\in T}\sum_{p\in P}\Big(C_p\big(g_{p,t}+C_p^R\big(r_{p,t}^{\uparrow}+r_{p,t}^{\downarrow}\big)\big)+SU_{p,t}C_p^{\mathrm{SU}}\Big)\\ &+\sum_{s\in S}\pi\sum_{t\in T}\sum_{p\in P}\big(C_p\big(a_{p,t,s}^{\uparrow}-a_{p,t,s}^{\downarrow}\big)+C^a\big(a_{p,t,s}^{\uparrow}+a_{p,t,s}^{\downarrow}\big)\big)\\ &+\sum_{s\in S}\pi\sum_{t\in T}\sum_{a\in A}\Big(s_{t,a,s}^{+}C^{\mathrm{s}}+s_{t,a,s}^{-}C^{\mathrm{d}}\Big) \qquad (1)\end{aligned}$$

A. First-stage constraints

The energy balance for the first stage is enforced by (2), while constraints relating to production limits, unit commitment and balancing capacity reservation are given in (3)-(6). Eq. (7) gives the grid constraints and specific hydropower constraints are defined by (8)-(13).

$$\sum_{p\in P_a^{area}} g_{p,t}+\sum_{l\in L_a} f_{l,t}=D_{a,t} \qquad (2)$$

where $t\in T$, $a\in A$

$$g_{pt}+r_{pt}^{\uparrow}\leq P_{max}b_{p,t} \qquad (3)$$

$$g_{pt}-r_{pt}^{\downarrow}\geq P_{min}b_{p,t} \qquad (4)$$

$$SU_{p,t}\geq b_{p,}-b_{p,t-1} \qquad (5)$$

$$b_{p,0}=0 \qquad (6)$$

where $t\in T$, $p\in P$

$$-F^{max}\leq f_{l,t}\leq F^{max} \qquad (7)$$

where $l\in L$, $t\in T$

$$v_{p0} = V_p^{init} \qquad (8)$$

$$q_{pt}^{in} = Q_{pt}^{nat}+\sum_{i\in I_p} q_{it}^{out} \qquad (9)$$

$$v_{p,t+1}-v_{pt} = q_{pt}^{in}-q_{pt}^{out} \qquad (10)$$

$$g_{pt} = E_p q_{pt}^{out} \qquad (11)$$

$$0\leq v_{pt}\leq V_p^{max} \qquad (12)$$

$$0\leq q_{pt}^{out}\leq Q_p^{max} \qquad (13)$$

where $p\in P^h$, $t\in T$.

B. Second-stage constraints

Similarly, (14)-(21) defines the constraints for the second stage. Except for also being indexed by scenario, the constraints for grid flow and hydropower are similar to the first, stage, so they are not included here. Notable aspects of the second-stage constraints are:

- Production in the energy balance is replaced with the sum of first-stage production and second-stage activation in (14) and the second stage energy balance is given in (15).
- Load shedding and production curtailment are limited by (16) and (17).
- Activation in the second stage is constrained by first-stage procurement of balancing capacity in (18) and (19).
- A balancing capacity buffer is procured in (20) and (21).

Previous research [8] has demonstrated that load shedding will be necessary in the continuous model if it follows the unit commitment decision of the discrete model without any modifications. To address this, constraints (20) and (21) incorporate a small buffer capacity requirement. These constraints ensure that each area reserves balancing capacity that exceeds the maximum activation needed across all scenarios.

For methodological consistency and to ensure both models have access to the same balancing capacity, we use a two-step approach:

1) The discrete model is first solved with all constraints.
2) It is then solved a second time with balancing capacity fixed to the results from the first step, but with constraints (20) and (21) removed.

$$\bar{g}_{pts} = g_{pt} + a^{\uparrow}_{pts} - a^{\downarrow}_{pts} \tag{14}$$

$$\bar{D}_{ats} = \sum_{p \in P^{area}_a} \bar{g}_{pts} + s^{+}_{tas} - s^{-}_{tas} + \sum_{l \in L_a} \bar{f}_{lts} \tag{15}$$

$$s^{+}_{tas} \leq \bar{D}_{ats} \tag{16}$$

$$s^{-}_{tas} \leq \sum_{p \in P^{area}_a} \bar{g}_{pts} \tag{17}$$

where $t \in T$, $a \in A$, $s \in S$

$$a^{\uparrow}_{p,t,s} \leq r^{\uparrow}_{pt} \tag{18}$$

$$a^{\downarrow}_{p,t,s} \leq r^{\downarrow}_{pt} \tag{19}$$

where $p \in P$, $t \in T$, $s \in S$.

$$\sum_{p \in P^{area}_a} r^{\uparrow}_{pt} \geq \sum_{p \in P^{area}_a} a^{\uparrow}_{p,t,s} + R^{\uparrow} \tag{20}$$

$$\sum_{p \in P^{area}_a} r^{\downarrow}_{pt} \geq \sum_{p \in P^{area}_a} a^{\downarrow}_{p,t,s} + R^{\downarrow} \tag{21}$$

where $t \in T, s \in S$

C. Continuous model

The continuous model only replaces the second stage of the discrete model. As illustrated by Fig. 1, first-stage production (g_{pt}) and reserve capacity ($r^{\uparrow}_{pt}/r^{\downarrow}_{pt}$) from the discrete model are taken as inputs and second-stage variables are replaced with Bernstein polynomials. We only include a brief description of the continuous-optimization methodology here, but a complete introduction can be found in Appendix C of [9].

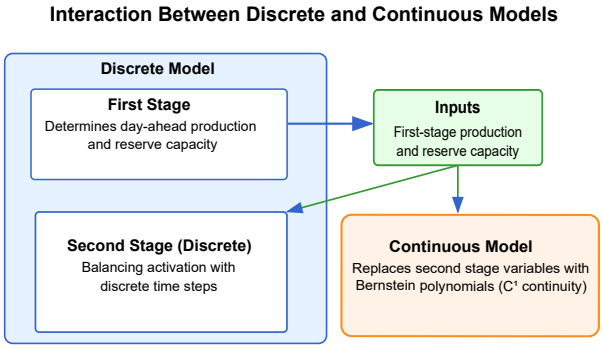

Fig. 1: Interaction between the discrete and continuous optimization models.

In continuous-optimization, a continuous variable $x(t)$ over a time period $[t_i, t_{i+1}]$, is represented using a weighted sum of Bernstein basis polynomials:

$$x(t) = \sum_{b \in B} w_{x,b} B_b(\tau(t)) \tag{22}$$

The Bernstein basis polynomials of degree n_B are defined as:

$$B_b(\tau) = \binom{n_B}{b} \tau^b (1-\tau)^{n_B - b} \tag{23}$$

This approach allows us to represent the continuous evolution of variables within each timestep, providing a C^1 continuous representation (i.e., with functions that are continuous and have continuous first derivatives) across the entire time horizon when appropriate continuity constraints are added.

The continuous model follows the same basic structure as the second stage of the discrete model, but reformulates constraints and variables to fit into a continuous framework. Constraints for hydropower and grid flow are modeled with constraints equivalent to (7)-(13), except indexes are added to denote scenario and Bernstein-weight. Similarly, continuous equivalent constraints are added for each of (14)-(17). The scenarios used in the continuous model corresponds directly to the ones used in the discrete model.

Second-stage production in the discrete model is constrained by equations (18) and (19). The continuous model must similarly respect these constraints while also maintaining C^1 continuity—a requirement that could create infeasibility. To address this challenge, we introduce an intermediate step that generates continuous approximations of the upper and lower production limits for each power plant. These approximations (denoted by parameters $\hat{P}^{max}_{ptsb}$ and $\hat{P}^{min}_{ptsb}$) are then used in equation (24) to constrain the second-stage production variables.

$$\hat{P}^{Min}_{ptsb} \leq \bar{g}_{ptsb} \leq \hat{P}^{Max}_{ptsb} \tag{24}$$

where $p \in P$, $t \in T$, $s \in S$ and $b \in B$.

To ensure C^1 continuity across timesteps on the production of each power plant, we add the following continuity constraints.

$$\bar{g}_{p,t,s,n_B} = \bar{g}_{p,t+1,s,0} \tag{25}$$

$$\bar{g}_{p,t,s,n_B} - \bar{g}_{p,t,s,n_B-1} = \bar{g}_{p,t+1,s,1} - \bar{g}_{p,t+1,s,0} \tag{26}$$

where $p \in P$, $t \in T \setminus \{|T|\}$, $s \in S$.

III. Case Study

A. System description

The test system consists of two areas: one hydro area and one thermal area. The hydropower system in the hydro area is based on the Nea-Nidelva watercourse. [10]. It consists of 12 reservoir-plant pairs, linked in a cascaded system, with a total production capacity of 535.3 MW. The hydro area follows the New York Independent System Operator (NYISO)

load profile for Hudson Valley from 01.01.2019 [11] as its target load profile. The thermal area uses 10 selected power plants, with a total production capacity of 735 MW, from the IEEE reliability test system [12] and follows the California Independent System Operator (CAISO) net load profile from 01.01.2019 [13]. These load profiles from the US have been selected because they have a time resolution of 5 minutes, which is higher resolution than most other publically available datasets. We assume that the load remains constant for the whole five-minute period. For both models, we distinguish between the target load and the model load:

- In the discrete model, the model load is obtained by averaging the target load over each model time step.
- In the continuous model, a Bernstein fitting tool is used to find load weights for each time step that best represent the target load.

To align peak demand with the available production capacity of the test system, the load time series are scaled so that the peak values are 580 (thermal area) and 510 (hydro area).

The second-stage scenarios are created by scaling the entire input load time series by a random multiplier, shifting the load curve up or down. The multiplier is sampled from a normal distribution with an expected value of 1 and a standard deviation of 0.1. A total of 10 scenarios were generated and used consistently for both the discrete and continuous models. Finally, the two areas are connected by a transmission line with a capacity of 200 MW.

B. Results

Fig. 2a presents the model load, target load, and the day-ahead scheduled production, each provided at a 60-minute temporal resolution. Since the first-stage production is the same for both models and all scenarios, it can differ significantly from the model load, which represents the actual demand the model must satisfy in a given scenario. The balancing adjustments required to transition from the day-ahead production to the model load are shown in Fig.2b.

The target load is the demand profile that the model load is based on. The figure clearly shows that the continuous model provides a better representation of the target load compared to the discrete model. The differences between the curves are plotted in Fig. 3. Although not displayed, both model load curves improve when moving to a 15-minute resolution.

The main takeaway from Fig. 2 is that while the continuous model will often have more balancing than the discrete model, the final production curve is closer to the target load, which leads to less remaining imbalance. This is supported by table I, which gives the total balancing activation and remaining imbalance for the discrete and continuous models using different time resolutions.

The 5-minute resolution column for the discrete model gives the best case scenario and serves as a benchmark for evaluating the other cases. Since the time resolution of the model load in this case exactly matches the target load, there are no remaining imbalances. In general, both total activation and remaining imbalances decrease with higher time resolution.

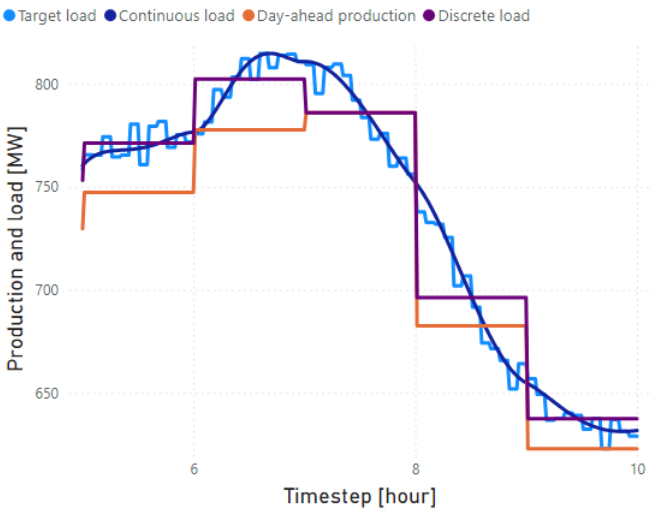

(a) Target load, model load for both models and first-stage production

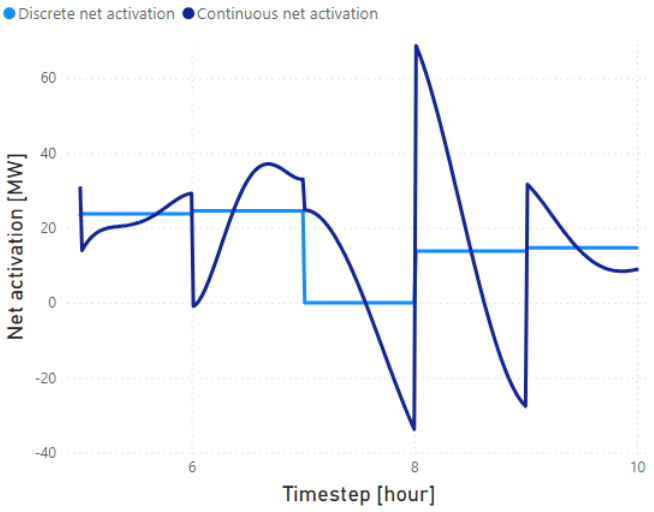

(b) Balancing activation to reach model load

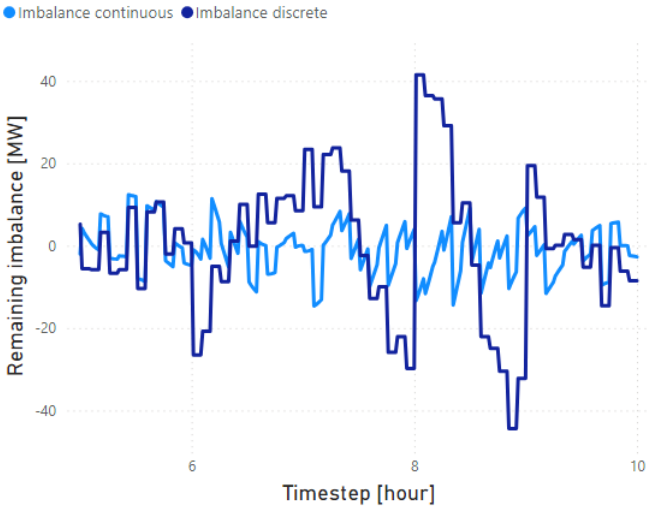

(c) Remaining imbalance between model load and target load

Fig. 2: Comparison between day-ahead production, model load and target load, along with model balancing and remaining imbalance for the system as a whole, from timestep 5-10.

Additionally, they are lower in the continuous model relative to the discrete model. Using the 60-minute discrete model as a base-case, and the 5-minute discrete model as a best-case, the 15-minute discrete model achieves about 60% of the possible reduction in activation. In contrast, the 60-minute continuous model achieves a 70% reduction, while the 15-minute continuous model reaches 84%.

TABLE I: Sum of up-activation, down-activation, and remaining imbalances for all scenarios and both areas

	Discrete			Continuous	
	60 min	**15 min**	**5 min**	**60 min**	**15 min**
Up-activation	7 478	7 953	7 866	7 488	7 943
Up-imbalance	1 724	699	-	497	282
Total up-activation	**9 202**	**8 652**	**7 866**	**7 985**	**8 225**
Down-activation	10 194	9 724	9 813	10 174	9 736
Down-imbalance	1 719	697	-	548	263
Total down-activation	**11 913**	**10 421**	**9 813**	**10 722**	**9 999**
Total	21 115	19 073	17 679	18 707	18 224

This difference in total activation arises because the models sometimes overshoot when balancing. If the target load is between the day-ahead production and the model load, the model will first activate balancing reserves to reach the model load, and then there will be a remaining imbalance in the opposite direction, causing the need for counterbalancing.

As previously mentioned, the target load used in this paper is based on CAISO for area 1 and NYISO for area 2. Fig. 3a shows a duration curve of the remaining imbalance in each of the four model variations for the CAISO target load and fig. 3b shows the same for the NYISO target load.

The characteristics of the target load determine much about the remaining imbalance. The CAISO (net-)load has a steep ramping during the morning and the evening, due to solar PV dominating midday production. This creates challenges for the discrete model, particularly in the 60-minute resolution case, resulting in large imbalances. In contrast, the continuous model performs much better under these conditions. Even the 60-minute resolution continuous model achieves lower imbalances than the 15-minute resolution discrete model, as seen in Fig. 3a.

The NYISO target load, on the other hand, is less affected by steep ramps but is more volatile in the short term. This volatility makes it harder for the continuous model to follow the load, making the advantage over the discrete model smaller.

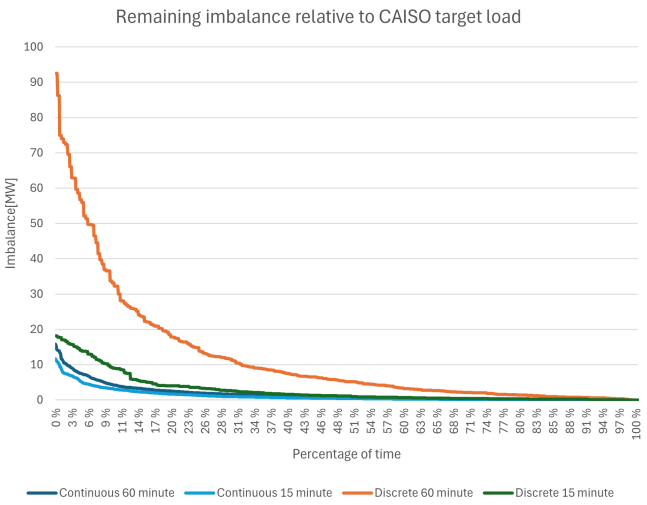

(a) Thermal area

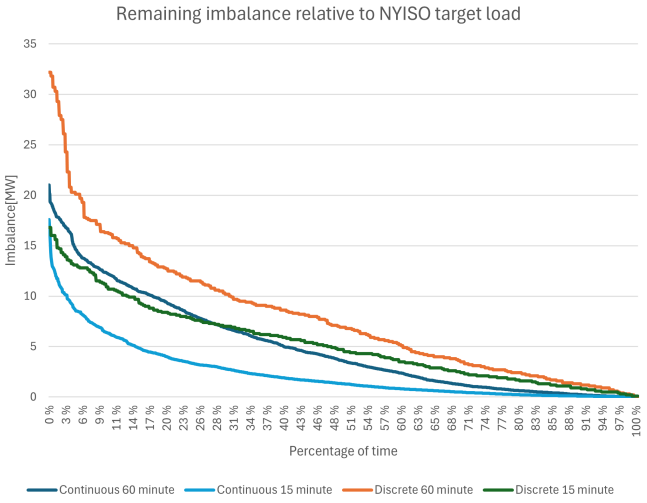

(b) Hydro area

Fig. 3: Duration curve showing the remaining imbalance in the thermal area relative to the target load, after the model load has been met

IV. Conclusion

In this paper, we show that higher temporal resolutions in optimization models lead to a better match between model load and target load. Similarly, employing a continuous optimization model instead of a discrete one improves the model load even further. This results in less remaining imbalances relative to the target load after balancing activation is done. In our case study, increasing the resolution from hourly to 15 minutes achieves about 60% of the possible reduction in total balancing, while switching to a continuous model reaches 84% of the possible reduction.

A continuous model like the one used in this paper could serve as a valuable tool for TSOs in planning ramping and balancing activation in power systems. By generating more predictable and realistic production schedules, this approach simplifies system balancing and has the potential to reduce remaining imbalances. This, in turn, minimizes frequency variations and enhances system resilience to disturbances.

Future work should refine this approach by incorporating different balancing reserve types (FCR, aFRR, mFRR) to provide insights into optimal resource management as balancing procedures evolve toward more proactive mFRR use and reactive aFRR responses.

REFERENCES

[1] Nordic Transmission System Operators. Solutions for a clean nordic energy system 2024–2030: Strategies to meet the climate and security challenge, August 2024.

[2] Nordic Balancing Model. Memo: Process for activating mfrr products, August 2024. Accessed: 2025-04-04.

[3] Jonas Bøe, Martin Håberg, and Gerard Doorman. Multi-area balancing energy activation optimization using entso-e standard products. In *2018 IEEE Power & Energy Society General Meeting (PESGM)*, pages 1–6. IEEE, 2018.

[4] Germán Morales-España, Andres Ramos, and Javier García-González. An mip formulation for joint market-clearing of energy and reserves based on ramp scheduling. *IEEE Transactions on Power Systems*, 29(1):476–488, 2014.

[5] Masood Parvania and Anna Scaglione. Unit commitment with continuous-time generation and ramping trajectory models. *IEEE Transactions on Power Systems*, 31(4):3169–3178, 2016.

[6] Kári Hreinsson, Bita Analui, and Anna Scaglione. Continuous time multi-stage stochastic reserve and unit commitment. In *2018 Power Systems Computation Conference (PSCC)*, pages 1–7, 2018.

[7] Christian Øyn Naversen, Arild Helseth, Bosong Li, Masood Parvania, Hossein Farahmand, and João P.S. Catalão. Hydrothermal scheduling in the continuous-time framework. *Electric Power Systems Research*, 189:106787, 2020.

[8] Mari Lund Øvstebø, Christian Øyn Naversen, Arild Helseth, and Hossein Farahmand. Continuous-time scheduling of a hydrothermal system with integration of offshore wind power. In *2020 17th International Conference on the European Energy Market (EEM)*, pages 1–6, 2020.

[9] Christian Øyn Naversen. *Modelling Approaches for Hydro-Dominated System Balancing*. PhD thesis, Norwegian University of Science and Technology, Trondheim, Norway, 2021.

[10] Norwegian Water Resources and Energy Directorate (NVE). Model of the norwegian hydropower system, 2024. Accessed: 2024-06-10.

[11] New York Independent System Operator. Load data nyiso, 2024. Accessed: 2024-12-09.

[12] Clayton Barrows, Jennie Jorgenson, Dheepak Krishnamurthy, Jessica Lau, Gordon Stephen, Jussi Ikaheimo, Eugene Preston, Andrea Staid, Jean-Paul Watson, Aaron Bloom, Brendan McBennett, and Matthew O'Connell. The ieee reliability test system: A proposed 2019 update. *IEEE Transactions on Power Systems*, 35(1):119–127, 2020. Publisher Copyright: © 1969-2012 IEEE.

[13] California Independent System Operator. Load data caiso, 2024. Accessed: 2024-12-09.